



Circular Polarization Observations of Type II Solar Radio Bursts and the Coronal Magnetic Field

R. Ramesh¹ , C. Kathiravan¹, and E. Ebenezer Chellasamy²¹ Indian Institute of Astrophysics, Koramangala 2nd Block, Bangalore 560034, Karnataka, India² Kodaikanal Solar Observatory, Indian Institute of Astrophysics, Kodaikanal 624103, Tamil Nadu, India

Received 2022 March 2; revised 2022 April 19; accepted 2022 May 8; published 2022 June 15

Abstract

It is well known that magnetic field strength (B) in the solar corona can be calculated using the Alfvén Mach number (M_A) and Alfvén speed (v_A) of the magnetohydrodynamic shock waves associated with coronal type II radio bursts. We show that observations of weak circularly polarized emission associated with the harmonic component of the type II bursts provide independent and consistent estimates of B . For the coronal type II burst observed on 2021 October 9, we obtained $B \approx 1.5$ G and ≈ 1.9 G at a heliocentric distance (r) of $\approx 1.8 R_\odot$, using the above two techniques, respectively.

Unified Astronomy Thesaurus concepts: Solar coronal mass ejections (310); The Sun (1693); Solar magnetic fields (1503); Solar radio emission (1522); Solar corona (1483)

1. Introduction

Most of the dynamical processes occurring in the solar corona are directly related to the magnetic field. Measurement of the latter is currently one of the widely pursued efforts in observational solar astronomy (see, e.g., Casini et al. 2017). Radio techniques are useful in this connection since field strengths can be measured both against the solar disk as well above the solar limb (see, e.g., White & Kundu 1997; Gelfreikh 2004 for observations in the “inner” corona, i.e., over $r \lesssim 1.1 R_\odot$). In the case of the “middle” corona ($1.1 R_\odot \lesssim r \lesssim 3.0 R_\odot$), observations of low-frequency ($\lesssim 100$ MHz) nonthermal radio bursts appear to be the potential tool at present. Though estimates using thermal radio emission from the “undisturbed” Sun are feasible, such observations are extremely rare and also require special circumstances (Kathiravan et al. 2002; Sastry 2009; Ramesh et al. 2021). The majority of the bursts are due to plasma processes (McLean & Labrum 1985). In the presence of a magnetic field, plasma emission propagates in two modes, i.e., ordinary (O) and extraordinary (X) modes, with opposite senses of rotation of the electric field vector. The propagation characteristics of these two modes in the solar corona are different. So there would be a resultant circular polarization (Melrose & Sy 1972; Ramesh et al. 2011b). The degree of circular polarization (dcp) is directly related to the strength of the magnetic field in the source, particularly in the case of harmonic plasma emission (Melrose et al. 1980). The polarization of the fundamental component is less straightforward but it also depends on the properties of the magnetic field. Hence observations of polarized radio bursts are a useful tool to estimate B . Several examples involving circularly polarized emission from harmonic type III bursts have been reported (Komesaroff 1958; Dulk & Suzuki 1980; Hanasz et al. 1980; Zlotnik 1981; Mercier 1990; Reiner et al. 2007; Ramesh et al. 2010c; Sasikumar Raja & Ramesh 2013b; Hariharan et al. 2014; Pulupa et al. 2020). In the present work, we focus on type II radio bursts from the solar corona since they are closely associated with CMEs (see, e.g.,

Aurass 1997; Lara et al. 2003; Cho et al. 2005; Gopalswamy et al. 2005; Lin et al. 2006; Gopalswamy 2006; Shanmugaraju et al. 2006; Cho et al. 2008; Gopalswamy et al. 2009; Ramesh et al. 2010b, 2012a; Gopalswamy et al. 2013; Zucca et al. 2014a; Kumari et al. 2019). The coronal magnetic field provides the energy that drives the CMEs. The bursts result from the excitation of plasma waves in the ambient medium due to nonthermal electrons accelerated by CME-driven MHD shock propagating outwards through the solar atmosphere. Radio spectral observations show the bursts as an intense narrow band of transient emission drifting slowly toward lower frequencies. The drift rate is typically < 1 MHz s^{-1} . The drift is due to the decrease of the electron density (N_e) in the solar atmosphere with increasing r . It is generally accepted that the radio waves are emitted near the local electron plasma frequency (f_p) and/or its harmonics. The corresponding emission in the spectra are called the fundamental (F) and harmonic (H) components of the type II burst. Sometimes, either or both the F and H bands of emission exhibit two branches, the lower-frequency branch (LFB) and the upper-frequency branch (UFB). Such events are called split-band type II bursts (see, e.g., Nelson & Melrose 1985 for details). It is well known that the Alfvén Mach number (M_A) and Alfvén speed (v_A) obtained from spectral observations of either the split-band structure or other characteristics exhibited by some of the type II radio bursts can be used to estimate B (Smerd et al. 1975; Vršnak et al. 2002; Gopalswamy & Yashiro 2011; Zucca et al. 2014b; Hariharan et al. 2015; Kishore et al. 2016; Kumari et al. 2017b, 2017c; Mancuso et al. 2019). There are reports that B can be obtained using observations of circularly polarized radio emission associated with the H-component of type II bursts also (Hariharan et al. 2014; Kumari et al. 2017a). We wanted to establish that the different radio methods involving type II radio bursts provide consistent estimates of B so that either or all of them could be used depending on the type of observational data available. Hence the present work.

2. Observations

The radio spectral data were obtained with the Kodaikanal solar observatory Radio Spectrograph (KRS; Indrajit et al. 2021) in the frequency range 85–35 MHz. It is a one-dimensional array



Original content from this work may be used under the terms of the [Creative Commons Attribution 4.0 licence](https://creativecommons.org/licenses/by/4.0/). Any further distribution of this work must maintain attribution to the author(s) and the title of the work, journal citation and DOI.

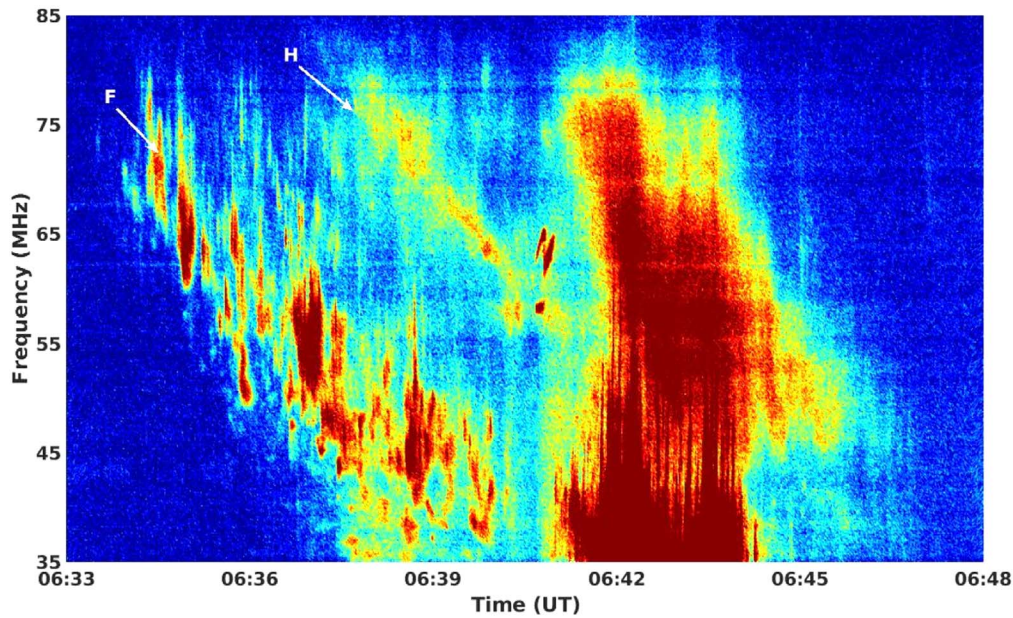


Figure 1. KRS dynamic spectra of type II and III radio bursts from the solar corona observed on 2021 October 9. The slower drifting emission in the interval $\approx 06:34$ – $06:40$ UT corresponds to a type II burst. The arrow marks indicate F and H bands in the burst. The faster drifting emission during the period $\approx 06:41$ – $06:45$ UT is a group of type III bursts.

of eight log-periodic dipole antennas (LPDA; Ramesh et al. 1998) set up along a north–south baseline. The half-power width of the response pattern (“beam”) of KRS for observations near the zenith is $\approx 90^\circ \times 6^\circ$ (R.A. \times decl.) at the highest frequency of operation, i.e., 85 MHz. While the width of the response pattern along R.A. is nearly independent of frequency, its width along the decl. varies inversely with the frequency. The observations were in the swept-frequency mode over the aforementioned frequency range with a sweep time ≈ 100 ms. The observing bandwidth at each frequency is ≈ 125 kHz. For polarization data, we used observations with the Gauribidanur Radio Interferometer Polarimeter (GRIP; Ramesh & Sastry 2005; Ramesh et al. 2008) at 80 MHz. The GRIP is operated by the Indian Institute of Astrophysics in the Gauribidanur Observatory (Ramesh 2011; Ramesh et al. 2014) located about 100 km north of Bangalore.³ It is an East–West one-dimensional interferometer array and observes the circularly polarized flux density from the “whole” Sun. Linear polarization, if generated at the corresponding radio source region in the solar atmosphere, gets canceled out in the corona itself due to the physical properties of the medium (Grognaard & McLean 1973; Morosan et al. 2022). The half-power width of the GRIP response pattern is broader compared to the Sun in both R.A. (≈ 1.5 at 80 MHz) and decl. ($\approx 90^\circ$). The latter is frequency independent. Thus, observations with the GRIP in the transit mode essentially reproduce its east–west “beam” at the observing frequency with amplitude proportional to the strength of the emission from the “whole” Sun at the corresponding frequency, weighted by the antenna gain in the corresponding direction. The two-dimensional radio images were obtained with the Gauribidanur Radioheliograph (GRAPH) at 80 MHz (Ramesh et al. 1998, 1999a, 2006b). The GRAPH is a T-shaped radio interferometer array of 384 LPDAs. Its angular resolution for observations close to the zenith is $\approx 4' \times 6'$ (R.A. \times decl.) at the above frequency. The integration time is ≈ 250 ms and the

observing bandwidth is ≈ 2 MHz. We also used data obtained with the Gauribidanur Low-frequency Solar Spectrograph (GLOSS; Ebenezer et al. 2001, 2007; Kishore et al. 2014; Hariharan et al. 2016b), Gauribidanur Radio Spectro-Polarimeter (GRASP; Sasikumar Raja et al. 2013a; Hariharan et al. 2015; Kishore et al. 2015; Mugundhan et al. 2018b), and e-CALLISTO (Monstein et al. 2007; Benz et al. 2009) to supplement KRS observations. For information on CMEs, we used the catalog generated from observations with the Large Angle and Spectrometric Coronagraph C2 (LASCO-C2; Brueckner et al. 1995) on board the Solar and Heliospheric Observatory (SOHO).⁴ We also used data obtained with the Extreme Ultra-Violet Imager (EUVI) which is part of the Sun–Earth Connection Coronal and Heliospheric Investigation (SECCHI; Howard et al. 2008) instruments on board the Solar Terrestrial Relations Observatory-A (STEREO-A).⁵

Figure 1 shows the dynamic spectrum of F–H type II burst observed with KRS on 2021 October 9. It is inhomogeneous and fragmented (see, e.g., Carley et al. 2021). The estimated shock speed from the burst assuming the widely used electron density model of Vrřnak et al. (2004) for the active region corona, is ≈ 1041 km s^{−1}. This is in good agreement with the corresponding value of ≈ 934 km s^{−1} reported from similar radio spectral observations elsewhere.⁶ The burst was associated with a 2B class H α flare from the sunspot region NOAA Active Region 12882 located at the heliographic coordinates N17E09. The flare was reported during the epoch $\approx 06:26$ – $07:22$ UT with a maximum at $\approx 06:38$ UT. There was also an M1.6 class GOES soft X-ray flare observed in the interval $\approx 06:19$ – $06:53$ UT with a maximum at $\approx 06:38$ UT. The SOHO/LASCO-C2 coronagraph observed a “halo” CME at $\approx 07:00$ UT with an angular width of $\approx 262^\circ$. The central position angle (CPA, measured counterclockwise from the

³ <https://www.iap.res.in/?q=centers/radio>

⁴ <https://wwwbis.sidc.be/cactus/catalog.php>

⁵ <https://cor1.gsfc.nasa.gov>

⁶ <https://ftp.swpc.noaa.gov/pub/warehouse/>

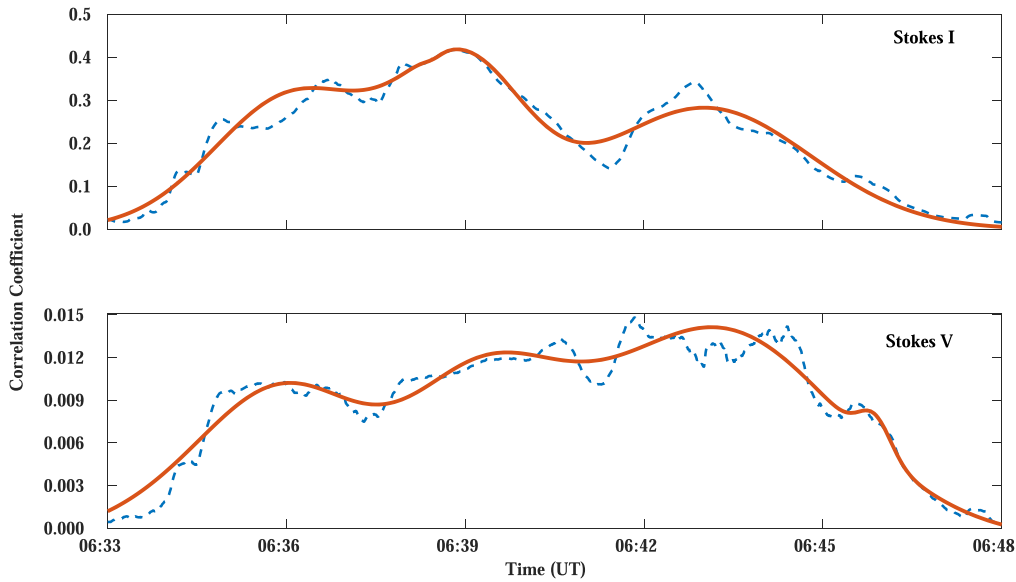


Figure 2. GRIP observations (at 80 MHz) of Stokes *I* and *V* emission associated with the different bursts in Figure 1. The dashed and thick lines in the upper and lower panels correspond to the observations and their fit, respectively. Emission in the period $\approx 06:37$ – $06:40$ UT corresponds to the H-component of the type II burst in Figure 1. The deflections during the epochs $\approx 06:34$ – $06:37$ UT and $\approx 06:41$ – $06:45$ UT relate to the F-component of the type II burst, and type III burst group in Figure 1, respectively.

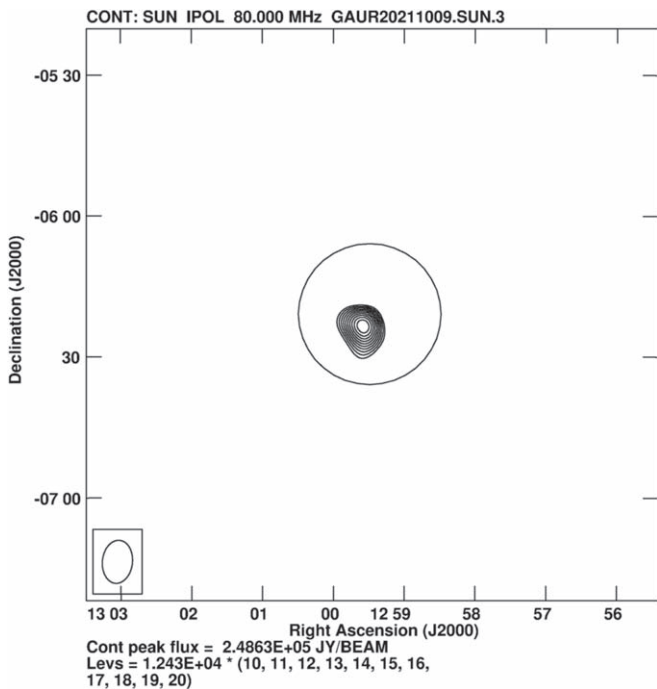


Figure 3. The 80 MHz GRAPH observations of the type II burst H-component in Figure 1 at $\approx 06:38$ UT. The circle indicates the extent of the solar photosphere. The inset near the lower-left corner represents the GRAPH “beam” at the above frequency. The data were calibrated using the standard Astronomical Image Processing System.

solar north) of the CME is $\approx 248^\circ$. The maximum speed of the CME is $\approx 844 \text{ km s}^{-1}$ in the plane of sky (POS). This is reasonably consistent with the type II burst shock speeds mentioned above considering that the deprojected speed of a “halo” CME whose associated source region is near the center of the solar disk is expected to be greater than the corresponding POS speed (see, e.g., Kathiravan & Ramesh 2004; Paouris et al. 2021). Note that speed estimates using radio spectral observations are independent of the source

location (see, e.g., Michalek et al. 2005). The average instantaneous bandwidth of the type II burst in Figure 1, estimated from its F-component, is ≈ 10 MHz. This indicates that the angular width of the associated CME should be $\approx 250^\circ$ (Ramesh et al. 2022). The latter is in good agreement with the CME observations mentioned above.

Figure 2 shows GRIP observations at 80 MHz, cotemporal with dynamic spectra in Figure 1. There is a noticeable Stokes *V* emission corresponding to the different bursts in Figure 1. The higher signal-to-noise ratio in the GRIP time profile at 80 MHz as compared to KRS spectra close to the above frequency is due to the better sensitivity of the former. For the present work, we concentrate on Stokes *I* and *V* emission corresponding to the H-component of the type II burst observed at $\approx 06:38$ UT. The observed peak correlation coefficients are ≈ 0.4 and ≈ 0.01 , respectively. The degree of circular polarization ($dcp = |V|/I$) is $\approx 3\%$. The corresponding value for the type III burst is $\approx 5\%$. This is consistent with the reports that type II bursts are weakly polarized (see, e.g., Komesaroff 1958; Stewart 1966; Suzuki et al. 1980), and radio techniques could be used to observe the associated low $dcp \sim 1\%$ (see, e.g., Kishore et al. 2015). Figure 3 shows two-dimensional imaging observations of the harmonic type II burst with GRAPH at $\approx 06:38$ UT. The observing frequency was 80 MHz, similar to GRIP. Note that at low frequencies, the observed position of a solar radio source could be different from its “true” position due to scattering by density inhomogeneities in the solar corona and/or refraction effects in the Earth’s ionosphere. But in the present case, the present observations were carried out during the transit of the Sun over the local meridian. Further, the zenith angle of the Sun in decl. (as observed from Gauribidanur) was less ($\approx 20^\circ$) on 2021 October 9. So any possible shift in source position due to the aforesaid effects is expected to be minimal at a frequency like 80 MHz, and also lesser than the angular resolution of the GRAPH mentioned in Section 2. (Riddle 1974; Stewart & McLean 1982; Mercier 1996; Ramesh et al. 1999b; Kathiravan et al. 2011; Ramesh & Ebenezer 2001b; Ramesh et al. 2011b, 2012b;

Mugundhan et al. 2016, 2018a). The estimated peak radio brightness temperature (T_b) from the GRAPH observations is $\approx 6.2 \times 10^8$ K. This is in the range of T_b values mentioned in the literature for the type II bursts at 80 MHz (see, e.g., Nelson & Robinson 1975).

3. Analysis and Results

Detailed calculations of the polarization of harmonic plasma emission imply that it should generally favor the O mode (Melrose et al. 1978), particularly for bursts with small dcp as in the present case (Willes & Melrose 1997). A statistical study of coronal type II bursts with herringbone structures by Suzuki et al. (1980) indicates that: (i) their polarization characteristics are the same as that of type II bursts without herringbones; (ii) the polarization of their H-component is similar to the polarization of the H-component of type III bursts. The latter corresponds invariably to the O mode (Dulk & Suzuki 1980). Therefore it is possible that the H-component of coronal type II bursts without herringbones as in the present case also correspond to O -mode polarization. We would like to add here that for harmonic plasma emission to be polarized in the O mode, the associated Langmuir waves should be parallel (within $\approx 20^\circ$) to the magnetic field (Dulk & Suzuki 1980). But reports of direct observations of Langmuir waves are rare. In one case study of an interplanetary type II burst, Graham & Cairns (2015) showed that the Langmuir waves are approximately one-dimensional and aligned with the magnetic field. Earlier, Bale et al. (1999) had reported similar observations of Langmuir waves upstream of a CME-driven interplanetary shock/type II burst. The shock accelerated electrons were first observed antiparallel to the interplanetary magnetic field and later parallel as well. Encouraged by the above reports, we used the following relation applicable for polarization of harmonic plasma emission to estimate B (Melrose et al. 1980; Zlotnik 1981):

$$dcp = \frac{11 f_B |\cos\theta|}{48 f_p} \quad (1)$$

where $f_B = 2.8 B$ is the gyrofrequency, f_p is the plasma frequency, and θ is the angle between the magnetic field direction and line of sight (LOS). Both f_B and f_p are in units of megahertz. In the present case, $dcp \approx 0.03$ and $f_p = 40$ MHz for the H-component of the type II burst (see Section 2). θ can be approximated to the heliographic longitude of the associated active region (see, e.g., Dulk & Suzuki 1980). This implies $\theta \approx 9^\circ$ in the present case (see Section 2). The angle between the centroid of the type II burst and LOS in Figure 3 is nearly the same ($\approx 11^\circ$). Using all the above values we find from Equation (1) that $B \approx 1.9$ G. Any possible center-to-limb variation is expected to be very minimal since the region is close to the center of the solar disk (see, e.g., Dulk & Suzuki 1980). Considering that the 40 MHz plasma level is located at $r \approx 1.79 R_\odot$ (see, e.g., Vrřnak et al. 2004), the B value in the present case corresponds to the above r . We would like to note here that the aforementioned location of the 40 MHz plasma level is in reasonable agreement with the corresponding values obtained from a statistical study of CMEs and type II bursts (Gopalswamy et al. 2013), and $5\times$ enhancement of N_e in the solar minimum “background” corona (Ramesh et al. 2006a). We verified the above result for

B using the definition,

$$B = 5.1 \times 10^{-5} v_A f_p \quad (2)$$

where $v_A = v_s/M_A$ is the Alfvén speed in kilometers per second, v_s is the shock speed, and M_A is the Alfvén Mach number. $v_s \approx 1041$ km s $^{-1}$ in the present case (see Section 2). We calculated M_A using STEREO-A/EUVI observations of the CME (mentioned in Section 2) associated propagating disturbance and the shock ahead of it. Applying the shock standoff distance technique (Gopalswamy & Yashiro 2011), we found that $M_A \approx 1.4$ during the type II burst interval in Figure 1. Note that the STEREO-A spacecraft was at $\approx E39^\circ$ during the corresponding epoch.⁷ The location of NOAA AR 12882 (see Section 2) therefore corresponds to $\approx 30^\circ$ in the western hemisphere for STEREO-A view. There are also reports that the average $M_A \approx 1.4$ in the “middle” corona (Smerd et al. 1974; Vrřnak et al. 2002; Kishore et al. 2016; Zucca et al. 2018). So, $v_A \approx 744$ km s $^{-1}$ in the present case. Substituting these values in Equation (2), we get $B \approx 1.5$ G. This is nearly equal to the estimated B using observed dcp of harmonic type II emission and Equation (1). Therefore the type II radio bursts are a versatile and complementary tool for the estimation of coronal magnetic field strength.

An inspection of Figure 2 reveals that the dcp of type II burst (F- and H-component) and type III burst group are all nearly equal, and small ($\approx 3\%–5\%$). The low dcp of type III bursts indicates that they are most likely H-component since F-component with $dcp < 10\%$ are rare (Suzuki & Sheridan 1978). The nearly equal dcp values of type II burst (F- and H-component) and type III burst (H-component) in Figure 2 suggest that the corresponding emission originates in the same region of the corona, and follows the same path in the corona also (see, e.g., Dulk et al. 1971). Note that in the case of type II bursts, reports indicate that the centroids of F- and H-components at any given observing frequency are nearly copatial (Zucca et al. 2018). So we can consider the corresponding emission to be generated in the same location, although there could be an apparent shift in the observed position of particularly the F-component due to propagation effects (Maguire et al. 2021). Moving further, depolarization as the cause of low dcp in the case of F-component O mode applies mostly to type I bursts only (see, e.g., Melrose 2017). Therefore the small values of dcp in the type II burst (F- and H-components) and type III bursts (H-component) in the present case are likely due to the escape of both O and X modes from the coronal plasma in the respective events (see, e.g., Fomichev & Chertok 1968). Coordinated observations with ground-based low-frequency radio facilities and Parker Solar Probe should possibly help to understand this better (see, e.g., Pulupa et al. 2020).

4. Summary

Measurement of the coronal magnetic field is one of the challenging problems in solar physics. In this situation, we have presented estimates of the field strength associated with the coronal type II radio burst (observed on 2021 October 9) using two different techniques and compared them for consistency. The burst was due to a “halo” CME with a source

⁷ https://stereo-ssc.nascom.nasa.gov/cgi-bin/make_where_gif

region near the center of the solar disk. From the observed circular polarization of the burst, we calculated $dcp \approx 0.03$ and $B \approx 1.9$ G at $r \approx 1.8 R_{\odot}$. In the case of the other often used a method involving v_A and M_A associated with coronal shock waves that excite type II bursts, the values obtained at the same r are $M_A \approx 1.4$, $v_A \approx 744 \text{ km s}^{-1}$, and $B \approx 1.5$ G. The close agreement between B in the two cases indicates that circular polarization of harmonic plasma emission from low-frequency radio bursts could be a useful supplementary tool to estimate the strength of the weak coronal magnetic field, particularly considering that measurements in the optical wavelengths are currently limited to the “limb” corona (see, e.g., Lin et al. 2004; Yang et al. 2020).

We express our gratitude to the Gauribidanur Observatory and Kodaikanal Solar Observatory staff members for their help in the observations and upkeep of the facilities. M. Rajesh and K. P. Santosh are acknowledged for their assistance with the present work. We thank the referee for the comments that helped us to describe the results more clearly.

ORCID iDs

R. Ramesh  <https://orcid.org/0000-0003-2651-0204>

References

- Aurass, H. 1997, in *Coronal Physics from Radio and Space Observations*, ed. G. Trottet (Berlin: Springer-Verlag), 135
- Bale, S. D., Reiner, M. J., Bougeret, J. L., et al. 1999, *GeoRL*, **26**, 1573
- Benz, A. O., Monstein, C., Meyer, H., et al. 2009, *EM&P*, **104**, 277
- Brueckner, G. E., Howard, R. A., Koomen, M. J., et al. 1995, *SoPh*, **162**, 357
- Carley, E. P., Cecconi, B., Reid, H. A., et al. 2021, *ApJ*, **921**, 3
- Casini, R., White, S. M., & Judge, P. G. 2017, *SSRv*, **210**, 145
- Cho, K.-S., Bong, S.-C., Kim, Y.-H., et al. 2008, *A&A*, **491**, 873
- Cho, K.-S., Moon, Y.-J., Dryer, M., et al. 2005, *JGRA*, **110**, A12101
- Dulk, G. A., Altschuler, M., & Smerd, S. F. 1971, *ApL*, **8**, 235
- Dulk, G. A., & Suzuki, S. 1980, *A&A*, **88**, 203
- Ebenezer, E., Ramesh, R., Subramanian, K. R., Sundara Rajan, M. S., & Sastry, C. V. 2001, *A&A*, **367**, 1112
- Ebenezer, E., Subramanian, K. R., Ramesh, R., Sundara Rajan, M. S., & Kathiravan, C. 2007, *BASI*, **35**, 111
- Fomichev, V. V., & Chertok, I. M. 1968, *SvA*, **12**, 21
- Gelfreikh, G. B. 2004, in *Solar and Space Weather Radiophysics*, ed. D. E. Gary & C. U. Keller (Berlin: Springer), 115
- Gopalswamy, N. 2006, in *Solar Eruptions and Energetic Particles*, ed. N. Gopalswamy, R. Mewaldt, & J. Torsti (Washington, DC: American Geophysical Union), 207
- Gopalswamy, N., Aguilar-Rodriguez, E., Yashiro, S., et al. 2005, *JGRA*, **110**, A12S07
- Gopalswamy, N., Thompson, W. T., Davila, J. M., et al. 2009, *SoPh*, **259**, 227
- Gopalswamy, N., Xie, H., Mäkelä, P., Yashiro, S., & Akiyama, S. 2013, *AdSpR*, **51**, 1981
- Gopalswamy, N., & Yashiro, S. 2011, *ApJL*, **736**, L17
- Graham, D. B., & Cairns, I. H. 2015, *JGRA*, **120**, 4126
- Grognard, R. J. M., & McLean, D. J. 1973, *SoPh*, **29**, 149
- Hanasz, J., Schreiber, R., & Aksenov, V. I. 1980, *A&A*, **91**, 311
- Hariharan, K., Ramesh, R., & Kathiravan, C. 2015, *SoPh*, **290**, 2479
- Hariharan, K., Ramesh, R., Kathiravan, C., Abhilash, H. N., & Rajalingam, M. 2016b, *ApJS*, **222**, 21
- Hariharan, K., Ramesh, R., Kishore, P., Kathiravan, C., & Gopalswamy, N. 2014, *ApJ*, **795**, 14
- Howard, R. A., Moses, J. D., Vourlidas, A., et al. 2008, *SSRv*, **136**, 67
- Indrajit, V. B., Kathiravan, C., Gireesh, G. V. S., et al. 2021, *SoPh*, **296**, 132
- Kathiravan, C., & Ramesh, R. 2004, *ApJ*, **610**, 532
- Kathiravan, C., Ramesh, R., Indrajit, V. B., & Rajalingam, M. 2011, *ApJ*, **730**, 91
- Kathiravan, C., Ramesh, R., & Subramanian, K. R. 2002, *ApJL*, **567**, L93
- Kishore, P., Kathiravan, C., Ramesh, R., Rajalingam, M., & Indrajit, V. B. 2014, *SoPh*, **289**, 3995
- Kishore, P., Ramesh, R., Hariharan, K., Kathiravan, C., & Gopalswamy, N. 2016, *ApJ*, **832**, 59
- Kishore, P., Ramesh, R., Kathiravan, C., & Rajalingam, M. 2015, *SoPh*, **290**, 2409
- Komesaroff, M. 1958, *AuJPh*, **11**, 201
- Kumari, A., Ramesh, R., Kathiravan, C., & Gopalswamy, N. 2017a, *ApJ*, **843**, 10
- Kumari, A., Ramesh, R., Kathiravan, C., & Wang, T. J. 2017b, *SoPh*, **292**, 161
- Kumari, A., Ramesh, R., Kathiravan, C., & Wang, T. J. 2017c, *SoPh*, **292**, 177
- Kumari, A., Ramesh, R., Kathiravan, C., Wang, T. J., & Gopalswamy, N. 2019, *ApJ*, **881**, 24
- Lara, A., Gopalswamy, N., Nunes, S., Muñoz, G., & Yashiro, S. 2003, *GeoRL*, **30**, 8016
- Lin, H., Kuhn, J. R., & Coulter, R. 2004, *ApJL*, **613**, L177
- Lin, J., Mancuso, S., & Vourlidas, A. 2006, *ApJ*, **649**, 1110
- Maguire, C. A., Carley, E. P., Zucca, P., Vilmer, N., & Gallagher, P. T. 2021, *ApJ*, **909**, 2
- Mancuso, S., Frassati, F., Bemporad, A., & Barghini, D. 2019, *A&A*, **624**, L2
- McLean, D. J., & Labrum, N. R. 1985, *Solar Radio Physics: Studies of Emission from the Sun at Metre Wavelengths* (Cambridge: Cambridge Univ. Press)
- Melrose, D. B. 2017, *RvMPP*, **1**, 5
- Melrose, D. B., Dulk, G. A., & Gary, D. E. 1980, *PASA*, **4**, 50
- Melrose, D. B., Dulk, G. A., & Smerd, S. F. 1978, *A&A*, **66**, 315
- Melrose, D. B., & Sy, W. N. 1972, *AuJPh*, **25**, 387
- Mercier, C. 1990, *SoPh*, **130**, 119
- Mercier, C. 1996, *AnGeo*, **14**, 42
- Michalek, G., Gopalswamy, N., & Yashiro, S. 2005, *AcA*, **55**, 151
- Monstein, C., Ramesh, R., & Kathiravan, C. 2007, *BASI*, **35**, 473
- Morosan, D. E., Räsänen, J. E., Kumari, A., et al. 2022, *SoPh*, **297**, 47
- Mugundhan, V., Ramesh, R., Indrajit, V. B., et al. 2016, *ApJ*, **831**, 154
- Mugundhan, V., Ramesh, R., Kathiravan, C., et al. 2018a, *ApJL*, **855**, L8
- Mugundhan, V., Ramesh, R., Kathiravan, C., Gireesh, G. V. S., & Hegde, A. 2018b, *SoPh*, **293**, 41
- Nelson, G. J., & Melrose, D. B. 1985, in *Solar Radiophysics: Studies of Emission from the Sun at Metre Wavelengths*, ed. D. J. McLean & N. R. Labrum (Cambridge: Cambridge Univ. Press), 333
- Nelson, G. J., & Robinson, R. D. 1975, *PASA*, **2**, 370
- Paouris, E., Vourlidas, A., Athanasios, P., & Anastasios, A. 2021, *SpWea*, **19**, e02617
- Pulupa, M., Bale, S. D., Badman, S. T., et al. 2020, *ApJS*, **246**, 49
- Ramesh, R. 2011, in *ASI Conf. Ser. 2, 1st Asia-Pacific Solar Physics Meeting*, ed. A. R. Choudhuri & D. Banerjee (Hyderabad: Astronomical Society of India), 55
- Ramesh, R., Anna Lakshmi, M., Kathiravan, C., Gopalswamy, N., & Umopathy, S. 2012a, *ApJ*, **752**, 107
- Ramesh, R., & Ebenezer, E. 2001b, *ApJL*, **558**, L141
- Ramesh, R., Kathiravan, C., Indrajit, V. B., Beeharry, G. K., & Rajasekara, G. N. 2010c, *ApJL*, **719**, L41
- Ramesh, R., Kathiravan, C., Indrajit, V. B., & Rajalingam, M. 2012b, *ApJ*, **744**, 165
- Ramesh, R., Kathiravan, C., & Satya Narayanan, A. 2011b, *ApJ*, **734**, 39
- Ramesh, R., Kathiravan, C., Sreeja, S. K., & Gopalswamy, N. 2010b, *ApJ*, **712**, 188
- Ramesh, R., Kathiravan, C., Sundara Rajan, M. S., Indrajit, V. B., & Rajalingam, M. 2014, in *ASI Conf. Ser. 13, The Metrewavelength Sky*, ed. J. N. Chengalur & Y. Gupta (Hyderabad: Astronomical Society of India), 19
- Ramesh, R., Kathiravan, C., Sundara Rajan, M. S., Indrajit, V. B., & Sastry, C. V. 2008, *SoPh*, **253**, 319
- Ramesh, R., Kathiravan, C., & Surya Natarajan, S. 2022, *ApJ*, **926**, 38
- Ramesh, R., Kumari, A., Kathiravan, C., Ketaki, D., & Wang, T. J. 2021, *GeoRL*, **48**, e91048
- Ramesh, R., Nataraj, H. S., Kathiravan, C., & Sastry, C. V. 2006a, *ApJ*, **648**, 707
- Ramesh, R., & Sastry, C. V. 2005, in *ASP Conf. Ser. 346, Large-scale Structures and their Role in Solar Activity*, ed. K. Sankarasubramanian, M. Penn, & A. Pevtsov (San Francisco, CA: ASP), 153
- Ramesh, R., Subramanian, K. R., & Sastry, C. V. 1999a, *A&AS*, **139**, 179
- Ramesh, R., Subramanian, K. R., & Sastry, C. V. 1999b, *SoPh*, **185**, 77
- Ramesh, R., Subramanian, K. R., Sundara Rajan, M. S., & Sastry, C. V. 1998, *SoPh*, **181**, 439
- Ramesh, R., Sundara Rajan, M. S., & Sastry, C. V. 2006b, *ExA*, **21**, 31
- Reiner, M. J., Fainberg, J., Kaiser, M. L., & Bougeret, J. L. 2007, *SoPh*, **241**, 351
- Riddle, A. C. 1974, *SoPh*, **35**, 153
- Sasikumar Raja, K., Kathiravan, C., Ramesh, R., Rajalingam, M., & Indrajit, V. B. 2013a, *ApJS*, **207**, 2
- Sasikumar Raja, K., & Ramesh, R. 2013b, *ApJ*, **775**, 38
- Sastry, C. V. 2009, *ApJ*, **697**, 1934

- Shanmugaraju, A., Moon, Y.-J., Cho, K.-S., Dryer, M., & Umapathy, S. 2006, *SoPh*, **233**, 117
- Smerd, S. F., Sheridan, K. V., & Stewart, R. T. 1974, in IAU Symp. 57, *Coronal Disturbances*, ed. G. A. Newkirk (Dordrecht: Reidel), 389
- Smerd, S. F., Sheridan, K. V., & Stewart, R. T. 1975, *ApL*, **16**, 23
- Stewart, R. T. 1966, *AuJPh*, **19**, 209
- Stewart, R. T., & McLean, D. J. 1982, *PASA*, **4**, 386
- Suzuki, S., & Sheridan, K. V. 1978, *R&QE*, **20**, 989
- Suzuki, S., Stewart, R. T., & Magun, A. 1980, in IAU Symp. 86, *Radiophysics of the Sun*, ed. M. R. Kundu & T. E. Gergely (Dordrecht: D. Reidel), 245
- Vršnak, B., Magdalenic, J., Aurass, H., & Mann, G. 2002, *A&A*, **396**, 673
- Vršnak, B., Magdalenic, J., & Zlobec, P. 2004, *A&A*, **413**, 753
- White, S. M., & Kundu, M. R. 1997, *SoPh*, **174**, 31
- Willes, A. J., & Melrose, D. B. 1997, *SoPh*, **171**, 393
- Yang, Z., Bethge, C., Tian, H., et al. 2020, *Sci*, **369**, 694
- Zlotnik, E. Y. 1981, *A&A*, **101**, 250
- Zucca, P., Carley, E. P., Bloomfield, D. S., & Gallagher, P. T. 2014a, *A&A*, **564**, A47
- Zucca, P., Morosan, D. E., Rouillard, A. P., et al. 2018, *A&A*, **615**, A89
- Zucca, P., Pick, M., Demoulin, P., et al. 2014b, *ApJ*, **795**, 68